Resonance Raman Scattering from Solutions of C_{60}

Sean H. Gallagher,[†] Robert S. Armstrong,*[,†] Wendy A. Clucas,[†] Peter A. Lay,*[,†] and Christopher A. Reed[‡]

School of Chemistry, University of Sydney, Sydney, New South Wales 2006, Australia, and Department of Chemistry, University of Southern California, Los Angeles, California 90089-0744

Received: January 16, 1997[⊗]

The resonance Raman (RR) spectrum of C_{60} has been studied in benzene and carbon disulfide using eight excitation wavelengths between 406.7 and 647.1 nm. Raman excitation profile calculations have been performed on the five most intense RR bands; the $H_g(1)$, $A_g(1)$, $G_g(4)$, $H_g(7)$, and $A_g(2)$ vibrational modes. Two main scattering mechanisms predominate, Herzberg−Teller (HT) B-term scattering and nonadiabatic D-term scattering. This is the first observation of rare D-term scattering in a system without a metal. The requirement of a Jahn−Teller distortion of the excited state, produced upon population of the degenerate T_{1u} LUMO, is essentially negated by solvent distortion of the symmetry of C_{60}. While the I_h point group is a good descriptor for the 10 fundamental Raman modes of C_{60}, the slight reduction in the high symmetry of the molecule, due to solvent and ^{13}C effects, activates at least 6 of the remaining 36 Raman-silent modes. At resonance with the HOMO−LUMO transition of C_{60}, or its vibronic sideband, the solution resonance Raman spectra of C_{60} display almost the full gamut of RR scattering phenomena with no fewer than 13 distinct classes of first- and second-order vibrational features. The intensity behavior and the depolarization ratio of the band due to the I_h-Raman-silent $G_g(4)$ mode at 1140 cm^{-1} suggest that the distorted excited state is best approximated as having D_{5d} symmetry. The presence of overtones and combinations of Raman-active and Raman-silent vibrational modes is explained in terms of a second-order HT scattering. These studies of the RR spectroscopy of C_{60} in solution have implications for the electron-pairing mechanism in the superconductivity of fullerides and the nature of solute−solvent associations such as between water-soluble derivatives of C_{60} and HIV-1 protease.

Introduction

Having I_h point-group symmetry, C_{60} is the most spherical molecule known to date. Beneath this beautiful simplicity and high symmetry, however, lies an elaborate network of coupled electronic and vibrational structure that can be most effectively probed by resonance Raman (RR) spectroscopy. Complicating this, the ground and excited state symmetries are sensitive to their solvent environments, resulting in distortions of the sphericity of the rapidly rotating C_{60}.[1,2]

Despite the extensive research into fullerenes in the last five years (>3000 papers), it is surprising that there are only a few papers on the resonance Raman scattering of C_{60}.[1,3−6] In the earliest two papers,[3,4] the discussion of the RR scattering behavior of C_{60} was limited to bands derived from the totally-symmetric A_g modes for C_{60}. In both of these studies the C_{60} samples were contaminated with C_{70}, which has three strong Raman bands (between 1446 and 1470 cm^{-1}) with large intensity enhancements at the excitation frequencies used in these experiments.[7] In another paper, McGlashen *et al.*[5] have described the use of RR spectroscopy to investigate the change in wavenumber of the band due to the $A_g(2)$ pentagonal pinch mode of C_{60} in solution upon reduction to C_{60}^{1-}. It was not until the HOMO−LUMO transition and its vibronic sideband were probed by us that substantial information on the resonance behavior of bands due to the non-totally-symmetric H_g modes was obtained.[1,6] The $H_g(7)$ vibrational mode at 1421 cm^{-1} receives intensity enhancement through rare D-term scattering, which arises from non-adiabatic vibronic coupling of the LUMO of C_{60} with the excited state of the higher energy C (3^1T_{1u}−1^1A_g) transition.[6] Most recently, a RR study of the spectrum of C_{60} in a number of solvents revealed that the symmetry of C_{60} is sensitive to its solvent environment, giving rise to a proliferation of bands arising from I_h IR-active/Raman-silent and I_h IR/Raman-silent vibrational modes.[1] Of the I_h IR/Raman-silent bands, the one that arises from the $G_g(4)$ mode at 1140 cm^{-1} has an intensity exceeded only by that of the most intense bands of Raman-active modes. This is remarkable and has significant implications for the symmetry of C_{60} in both the ground and excited states. Lynch *et al.*[8] have also reported additional bands in the nonresonant FT-Raman solution spectra of C_{60}. They propose that these bands originate from isomers of C_{60}.[8,9] This is disputed as such an assertion is inconsistent with other experimental evidence and is addressed elsewhere.[10]

Bands due to higher-order Raman modes have been reported previously in measurements conducted on thin films of C_{60}.[11] However, here, as elsewhere in the literature, interpretations of these Raman experiments are inadequate[12] because authors have neglected the possibility of resonance enhancement from excitation in the region of the forbidden electronic transitions (488.0 and 514.5 nm).[11,13−19] In contrast, Bowmar *et al.*[20] reported a "weak resonance" at these laser excitations for both solvated and unsolvated C_{60} crystals.

In this paper, we present the Raman excitation profiles (REPs) at seven laser wavelengths between 514.5 and 406.7 nm for the five most intense Raman bands of C_{60} in solution, due to the $H_g(1)$, $A_g(1)$, $G_g(4)$, $H_g(7)$, and $A_g(2)$ vibrational modes. The REPs provide invaluable information on the different light-scattering mechanisms that operate, on the nature of the resonant electronic excited states, and on the nature of the vibrational modes. These also have implications for two interesting applications of C_{60}—the superconductivity of fullerides and the

[†] University of Sydney.
[‡] University of Southern California.
[⊗] Abstract published in *Advance ACS Abstracts,* March 15, 1997.

S1089-5639(97)00232-6 CCC: $14.00

inhibition of HIV-1 protease by water-soluble derivatives of C_{60}. Electron−phonon coupling with electrons in the LUMO of C_{60} is fundamental to superconductivity,[21−23] and there is still much to be learned about the intermolecular interactions of C_{60}.

Experimental Section

The resonance Raman spectra were obtained using two lasers. A Spectra Physics 2025-11 CW krypton ion laser provided the violet lines at 406.7 and 413.1 nm, and the red line at 647.1 nm. A Spectra Physics 2025-05 CW argon ion laser provided five blue-green lines at 457.9, 476.5, 488.0, 496.5, and 514.5 nm. Typical laser power was 20−150 mW, depending on the power available for the excitation wavelength. The scattered light was focused with a Leitz f1.0 lens and collected at a 90° scattering geometry from the quartz spinning cell (∼2000 rpm). A polarization scrambler was used in all experiments to correct the polarization bias of the Jobin-Yvon U1000 double monochromator (1800 grooves/mm gratings). Slit settings were 300 μm for all experiments. Calibration of the monochromator was performed using the mercury emission lines of the fluorescent lights in the laboratory. FT-Raman spectra were recorded on a Bruker RFS 100 spectrometer with 1064-nm Nd:YAG laser excitation using a 1-cm path length cuvette.

Saturated solutions of C_{60} (MER Corporation (Texas) >99.9%) were prepared in CS_2 (Merck, >99.9%) and benzene (Merck, >99.5%). Two types of RR experiments were performed. The REP experiments were the average of four runs at each wavelength, for C_{60} in benzene, with 2-s integration times at each datum collection point between 200 and 1600 cm^{-1}. The second experiment recorded the RR spectrum of C_{60} in CS_2 between 200 and 3000 cm^{-1} using 413.1-nm excitation. Collection was completed for four scans at 4-s integration times in ∼200-cm^{-1} regions. This was required to minimize the photodecomposition of CS_2 in the laser beam, which caused some fluorescence at wavenumbers above 1700 cm^{-1}. The resultant spectrum (resolution of ±1 cm^{-1}) was then taken from the average of all scans after ensuring that there was no observable decomposition of C_{60} over the time scale of each experiment. All resonance Raman plots are uncorrected for base line, and no smoothing has been performed on the spectra. Depolarization ratios were obtained using a polarizing filter aligned either parallel or perpendicular to the electric vector of the scattered light. FT-Raman spectra were recorded, at 1.5-cm^{-1} resolution for 4096 scans, for the same C_{60} concentration in CS_2 solution as was used in the RR experiments. The power at the sample was 200 mW. To obtain the intensities and deconvolutions of Raman bands, fits to band areas were performed using a GRAMS/386-based package.[24]

The REP calculations involved normalizing all Raman band scattering intensities across the absolute energy range (cm^{-1}). The first correction involved the "ν^4" correction for the dependence of the intensity of the Raman band on the fourth power of the absolute energy. This was performed by comparing the benzene solvent band at 605 cm^{-1} with the $H_g(1)$ band at 264 cm^{-1} and the $A_g(1)$ band at 490 cm^{-1}, and the solvent band at 1568 cm^{-1} with the $G_g(4)$, $H_g(7)$, and $A_g(2)$ vibrational bands at 1140, 1421, and 1468 cm^{-1}, respectively. Equation 1 was used to calculate this effect

$$R_1 = \frac{(E_L - E_S)^4}{(E_L - E_V)^4} \quad (1)$$

where E_L is the energy of the laser line, E_S is the energy of the reference solvent band, and E_V is the energy of the C_{60} Raman band. They are all calculated in absolute wavenumber (cm^{-1}),

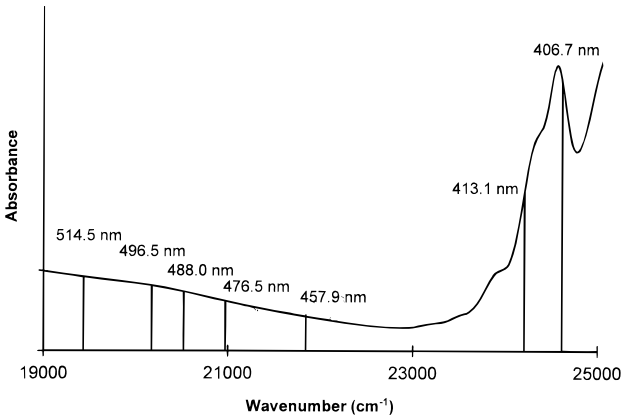

Figure 1. Positions of the laser excitation energies relative to the electronic absorption spectrum of C_{60} in benzene.

rather than the relative wavenumber compared to the excitation energy. The raw band intensities were then multiplied by R_1. The next correction was required to account for the spectral response of the photomultiplier tube (PMT). Light from a halogen quartz lamp, rated at 3150 K at 3.000 A, was scattered off a MgO-coated surface through the focusing lens and polarization scrambler into the monochromator. The spectral response of the PMT was measured between 12 500 and 24 500 cm^{-1}. This produced a curve that was divided into the predicted curve for radiation of a blackbody at 3150 K.[25] The quotient was a function that yielded a ratio, R_2, at each energy division. Each band intensity was then multiplied by R_2. The final correction accounted for self-absorption and differences in the optical path length in each experiment. This was achieved by normalizing the nonresonant intensities of the reference solvent bands at 605 and 1586 cm^{-1} for all excitation wavelengths relative to the intensities of these bands measured at 488.0 nm. All band energies were then scaled relative to these solvent bands to give the final intensity of the Raman bands.

Results

The data obtained from different solvents showed similar trends, and the frequencies and intensities of each band were the same, within experimental error, in different solvents, except for those arising from 413.1- and 406.7-nm excitations. The positions of each of the laser lines relative to the electronic absorption spectrum of C_{60} in benzene are given in Figure 1, and typical RR spectra of C_{60} in benzene are shown in Figure 2. The REPs at the laser excitation wavelengths of 514.5, 496.5, 488.0, 476.5, 457.9, 413.1, and 406.7 nm for the bands due to the $H_g(1)$, $A_g(1)$, $G_g(4)$, $H_g(7)$, and $A_g(2)$ vibrational modes of C_{60} at 264, 490, 1140, 1421, and 1468 cm^{-1}, respectively, are presented in Figure 3. The most notable result is the greater intensity of the bands of these five Raman modes at 413.1- and 406.7-nm excitation. In general, the highest intensity of each band occurs at 413.1 nm, except for the bands arising from the $H_g(7)$ vibrational mode, which has its greatest intensity at 406.7 nm. Table 1 gives the ratios of the band intensities at 406.7 and 413.1 nm and at 514.5 and 413.1 nm and the depolarization ratios for each band. In the region 514.5−457.9 nm, the $H_g(1)$ and $A_g(1)$ vibrational bands have the highest intensities relative to their maximum band intensities, at 0.55 and 0.27, respectively. The $A_g(2)$ vibrational mode gives rise to a band that has a lesser relative intensity in this region at 0.05 of its peak intensity at 413.1 nm, while the $G_g(4)$ and $H_g(7)$ vibrational band intensities are negligible in this region. Bands due to fundamental modes of C_{60} in CS_2 solution in the FT-Raman experiment (normal Raman) were very weak in intensity in comparison to solvent

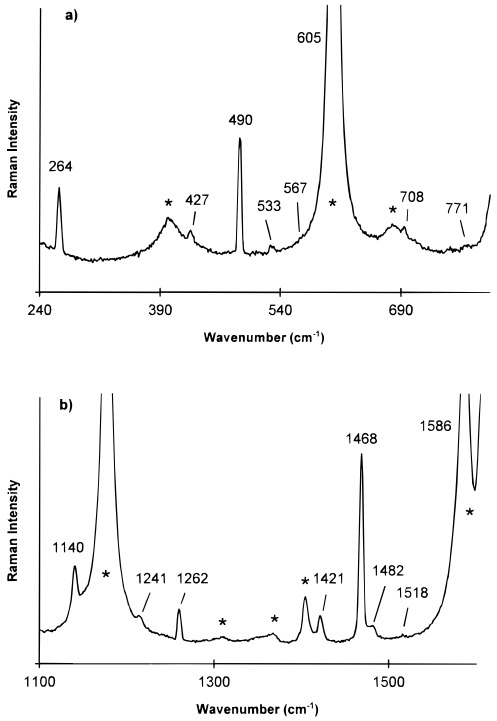

Figure 2. (a) RR spectrum of C_{60} in benzene at 413.1-nm excitation for the wavenumber region 240−750 cm^{-1}. (b) RR spectrum of C_{60} in benzene at 413.1-nm excitation for the wavenumber region 1000−1650 cm^{-1}. The band at 1262 cm^{-1} is a mercury emission line from fluorescent lights for calibration. Solvent peaks are asterisked.

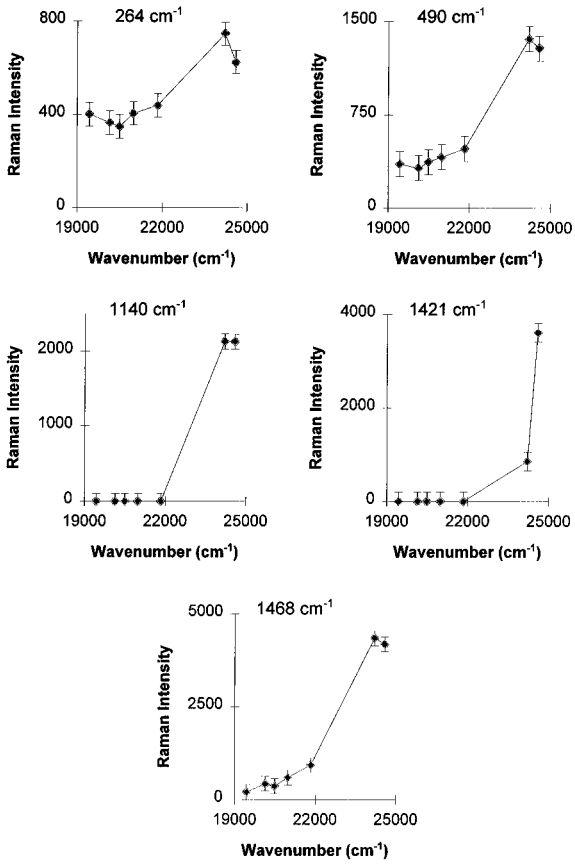

Figure 3. Raman excitation profiles constructed for 264, 490, 1140, 1421, and 1468-cm^{-1} bands of C_{60} in benzene at the seven laser lines in Figure 1.

bands. This showed that, at resonance, the intensity enhancement of the bands due to the Raman fundamental modes of C_{60} is at least 2 orders of magnitude greater relative to solvent bands.

TABLE 1: Ratio of the Band Intensities and Depolarization Ratios[a] for the Most Intense Resonance Raman Modes of C_{60} at 0−1 and 0−0 Resonances[b] and at 514- and 413-nm Resonances

	$H_g(1)$	$A_g(1)$	$G_g(4)$	$H_g(7)$	$A_g(2)$
I_{0-1}/I_{0-0}	0.84	0.95	1.00	4.23	0.96
I_{514}/I_{413}	0.55	0.27	0.00	0.00	0.05
$\rho(\pi/2)$	0.73	0.00	0.60	0.50	0.05

[a] Depolarization ratios $\rho(\pi/2)$ for each band are based on the intensities for perpendicular and parallel electric field vectors. The depolarization experiments were performed at 413.1-nm excitation for C_{60} solutions in CS_2. The errors in $\rho(\pi/2)$ are ±0.05. [b] The errors in the intensity ratios are ±20% as the relative positions of the laser lines with respect to the maximum absorbance of the respective transitions must be considered.

TABLE 2: Assignment of RR Bands of C_{60} in CS_2 and Benzene[a]

fundamental mode	wavenumber (cm^{-1})	combinations and overtones	wavenumber[a] (cm^{-1})
$H_g(1)$	264	$A_g(1) + H_g(2)$	913 (4)
$H_g(2)$	427	$2A_g(1)$	980 (0)
$A_g(1)$	490	$A_g(1) + T_{1u}(1)$	1020 (3)
$T_{1u}(1)$	533	$A_g(1) + T_{2u}(2)$	1184 (0)
$T_{1u}(2)$	567	$A_g(1) + H_g(3)$	1195 (3)
$T_{2u}(2)$	694	$A_g(1) + G_u(3)$	1349 (0)
$H_g(3)$	708	$A_g(1) + H_g(5)$	1582 (0)
$H_g(4)$	771	$A_g(1) + G_g(4)$	1630 (0)
Gu(3)	860	$A_g(2) + H_g(1)$	1736 (4)
$H_g(5)$	1100	$H_g(3) + G_g(4)$	1852 (0)
$G_g(4)$	1140	$A_g(2) + H_g(2)$	1896 (1)
$T_{1u}(3)$	1189	$A_g(1) + H_g(7)$	1913 (2)
$H_g(6)$	1241	$A_g(1) + A_g(2)$	1961 (3)
$H_g(7)$	1421	$2G_g(4)$	2283 (3)
$A_g(2)$	1468	$G_g(4) + T_{1u}(3)$	2327 (2)
$H_g(8)$	1570	$H_g(7) + G_g(4)$	2564 (3)
		$A_g(2) + G_g(4)$	2608 (0)
		$2H_g(7)$	2845 (3)
		$A_g(2) + H_g(7)$	2891 (2)
		$2A_g(2)$	2940 (4)

[a] The difference between calculated and experimental values for the combinations and overtones appears in parentheses.

The RR spectra of C_{60} in CS_2 have at least 26 bands other than those attributable to the 10 fundamental Raman-active modes. These results are summarized in Table 2, along with band assignments. The difference between the sum of the energies of the contributing bands and the energy of the bands due to the combination/overtone modes, based on the harmonic approximation, is shown in brackets. In most cases, the difference is 2 cm^{-1}, and at most is 4 cm^{-1}. These bands belong to 13 distinct classes of first- and second-order scattering phenomena from vibrations in I_h symmetry, organized in these categories:

totally-symmetric Raman-active modes
non-totally-symmetric Raman-active modes
infrared-active and Raman-silent modes
Raman- and infrared-silent modes
overtones of totally-symmetric modes
overtones of non-totally-symmetric modes
overtones of IR/Raman-silent modes
combinations of totally-symmetric modes
combinations of totally- and non-totally-symmetric modes
combinations of totally-symmetric and infrared-active modes
combinations of totally-symmetric and IR/Raman-silent modes
combinations of non-totally-symmetric and IR/Raman-silent modes
combinations of infrared-active and IR/Raman-silent modes

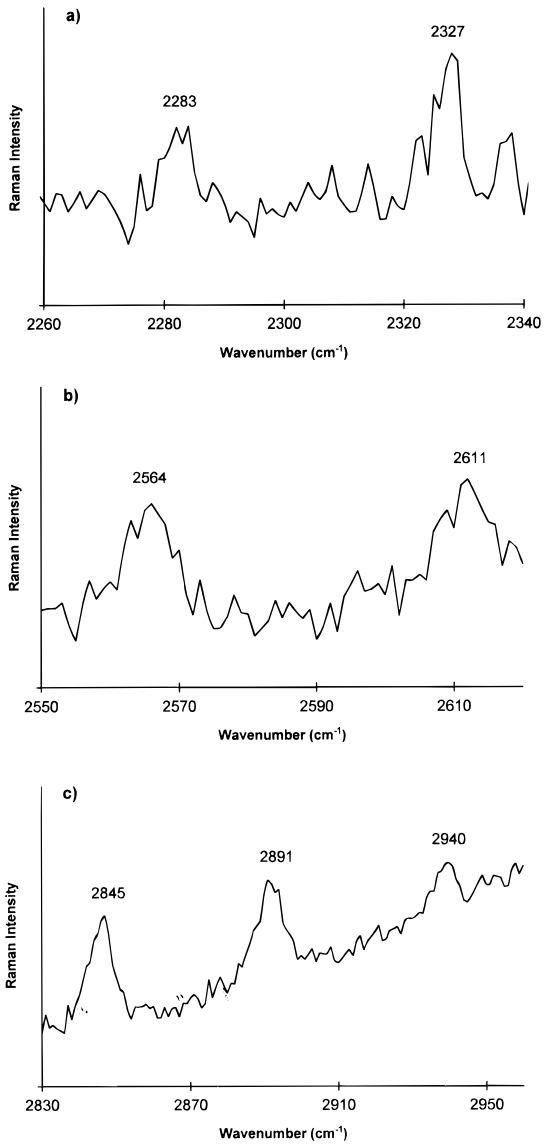

Figure 4. Selected wavenumber regions of the CS_2 solution RR spectrum of C_{60}. (a) $2G_g(4)$ overtone and $G_g(4) + T_{1u}(3)$ combination mode at 2283 and 2327 cm^{-1}, respectively. (b) $H_g(7) + G_g(4)$ and $A_g(2) + G_g(4)$ combination modes at 2564 and 2608 cm^{-1}, respectively. (c) $2H_g(7)$ and $2A_g(2)$ overtones at 2845 and 2940 cm^{-1}, respectively, and $H_g(7) + A_g(2)$ combination mode at 2891 cm^{-1}.

These results include the unusual observation of the band due to an overtone of an infrared- and Raman-silent mode, *i.e.*, the $2G_g(4)$ mode giving rise to the band at 2283 cm^{-1}. The $G_g(4)$ mode is also involved in a combination of totally-symmetric and IR/Raman-silent modes for the bands due to the $A_g(2) + G_g(4)$ mode at 2608 cm^{-1}, non-totally-symmetric and silent modes for the $H_g(7) + G_g(4)$ mode at 2564 cm^{-1}, and infrared-active and IR/Raman-silent modes for the $T_{1u}(3) + G_g(4)$ combination at 2327 cm^{-1}. These results are given in Figure 4.

Discussion

Since all excitation wavelengths, except that used for the FT-Raman, produced RR spectra, only RR scattering mechanisms need be considered in detail. C_{60} displays 13 classes of RR scattering phenomena, probably more than any other individual molecule, complex, or ion. Recently, we have shown that vibronic coupling[6] and solvent distortion of the sphericity of C_{60}[1] are integral to the molecule's RR behavior. In a solvent

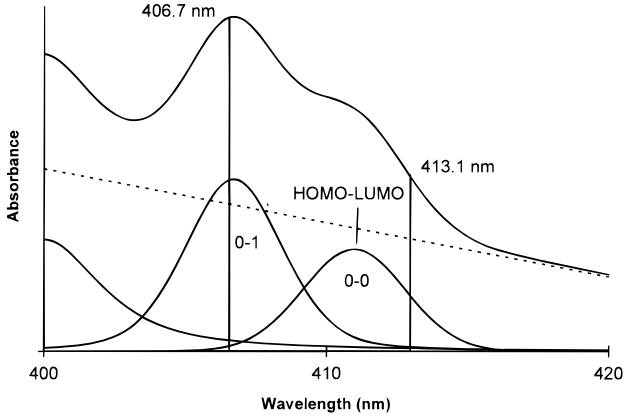

Figure 5. Deconvolution of the electronic spectrum of C_{60} in the region 400−420 nm showing the position of the 413.1- and 406.7-nm laser lines relative to the A electronic state. The 0−0 band is due to the origin transition, and the 0−1 band is due to the first vibronic transition involving the $H_g(1)$ mode. The dashed line represents the base line used in the deconvolution.

environment, the fast rotation of C_{60} is slowed in electron-donating solvents, such as aromatics. This increases the effective rotating volume and thereby results in a dynamic distortion of the ball.[2] This symmetry reduction mechanism is postulated to have a greater effect than that due to ^{13}C splitting.[1] The lowering of symmetry relaxes the Raman selection rules and allows for the proliferation of scattering phenomena in the RR spectrum of C_{60}. This is significant because, unlike most molecules, only slight distortions to the high symmetry of C_{60} relax the Raman selection rules and the vibrations involve only small nuclear displacements of individual atoms (see below). Also, the intensity enhancement mechanisms of both the Raman-active and Raman-inactive modes reveal the complicated nature of the vibronic network that couples the resonant excited state with other excited states.

The electronic spectrum of C_{60} can be separated into two spectral regions. The 190−410 nm region consists mainly of the spin- and symmetry-allowed singlet−singlet transitions, whereas at wavelengths >410 nm forbidden transitions dominate the spectrum.[26] As C_{60} belongs to a icosahedral point group, all allowed electronic transitions will have the same symmetry. Two of these transitions are important in this work: the weak HOMO−LUMO is the origin transition of the A electronic state ($1^1T_{1u}-1^1A_g$, $f = \sim 0.015$)[26] at ~410 nm and the more strongly-allowed C transition, the $3^1T_{1u}-1^1A_g$ ($f = 0.37$) at ~330 nm. The band due to the $1^1T_{1u}-1^1A_g$ (0−0) transition has sidebands of at least six HT-activated vibronic transitions (0−1), starting with the $1^1T_{1u}-1^1A_g + H_g(1)$ at ~406 nm.[26] The A electronic state is probed by the 413.1- and 406.7-nm lines, which are in resonance with the 0−0 and 0−1 ($H_g(1)$) transitions, respectively, as illustrated in Figure 5. This region of the electronic spectrum of C_{60} is analogous to the Soret (B) and Q bands of metalloporphyrins and is similar in appearance. Hence, the scattering mechanisms responsible for the rich nature of the RR spectra of the metalloporphyrins[27] are also likely to be relevant in the RR activity of C_{60}. Three of these light-scattering mechanisms operate for C_{60} and are discussed below. For a schematic representation of the Herzberg−Teller and nonadiabatic scattering mechanisms, see ref 30.

The forbidden electronic transition region of C_{60} gains intensity through Herzberg−Teller interactions, in which excitation of a vibration of suitable symmetry enables a forbidden electronic transition to borrow intensity from an allowed electronic transition.[28] Leach *et al.*[26] have assigned the electronic absorption in the region of investigation in this work to

the forbidden singlet−singlet transition $1^1H_u-1^1A_g$. The origin transition, ϵ_0, for this state occurs at 526.0 nm in *n*-hexane followed by 0−1 vibronic sidebands comprised of at least three transitions, the ϵ_1 ($\epsilon_0 + A_g(1)$) at ∼510 nm, the ϵ_2 ($\epsilon_0 + G_g(?)$) (sic) at ∼502 nm, and the ϵ_3 ($\epsilon_0 + H_g(6)$) at ∼496 nm.

The intensity profiles of the RR bands in Figure 3 essentially follow the absorption profile of C_{60} across the region 406.7−514.5 nm; *i.e.*, they have greater intensity upon resonance with the A electronic state and weaker intensities upon resonance with the forbidden transitions. The following discussion of the REP of C_{60} in this region observes this distinction and so treats resonance with the A electronic state and resonance with the forbidden transitions, the ϵ electronic state, separately.

Resonance with the A Electronic State. For totally-symmetric modes, A-term scattering usually dominates and generally has the largest contribution to the intensity of the bands in the RR spectra.[28−30] If, however, the resonant electronic transition is only weakly-allowed and the Franck−Condon factors are correspondingly small, as for the HOMO−LUMO transition in C_{60}, then the A-term scattering contribution will be essentially negligible.[28−30] This can be understood in terms of the structures of fullerenes. Fullerenes are unlike most other classes of molecules owing to their rigid three-dimensional cage structures. Vibrationally, this is important as there are no discrete vibrating units; the only gross delineation of vibrational modes of fullerenes is their tangential or radial nature. This connectivity of the fullerene frame is also important for their resonance Raman scattering. Vibrational modes that have the same vibrational coordinates as the displacement of the molecular geometry in the excited state will have their band intensities enhanced by A-term scattering. The nuclear displacement, ΔQ, of the potential surface of the excited electronic state minimum from that of the ground electronic state is defined as

$$\Delta Q = \mu^{1/2}\Delta S \tag{2}$$

where μ is the reduced mass associated with the vibration and ΔS is the corresponding displacement along the relevant symmetry coordinates. It is related to the change in bond lengths, Δr, by

$$\Delta S = \frac{1}{\sqrt{n}}(\Delta r_1 + ... + \Delta r_n) \tag{3}$$

where n is the number of bonds involved with the vibration. Since n is large and Δr is small, A-term scattering will be very weak and much less important than B-term scattering for fullerenes. B-term scattering (Herzberg−Teller scattering) thus will be the major source of intensity enhancement of scattering for non-totally-symmetric modes and also for totally-symmetric modes when A-term scattering is weak.[28−30]

The B-term enhancement of Raman band intensity of a vibrational mode is dependent upon two factors. These factors are the efficacy of the vibrational mode to couple the electronic excited states, as indicated from group theory considerations and the nature of the changes in the electron density upon excitation relative to the vibrational mode coordinates. Hence, B-term scattering explains why vibrational modes of the same symmetry sometimes have different excitation profiles. Considerations of symmetry reduction are also important for solution RR studies of C_{60}.[1]

All excited states of allowed electronic transitions of C_{60} have T_{1u} symmetry. Vibrations that couple these electronic excited states are found using group theory in the symmetric part of the direct product involving T_{1u}:

$$T_{1u} \otimes T_{1u} = A_g + [T_{1g}] + H_g \tag{4}$$

Hence, upon resonance with the A electronic state, the Raman-active modes of C_{60} are capable of coupling the T_{1u} excited state of the LUMO with the T_{1u} excited states of higher energy transitions. The bands of the vibrational modes that couple the electronic states borrow intensity from the higher energy electronic excited state and have their intensities enhanced in the RR spectrum, as evidenced by the presence of all 10 Raman-active vibrational modes. The band intensities corresponding to the H_g modes at 427, 708, 771, 1100, and 1241 cm^{-1}, however, are weak suggesting that the molecular motion of these modes is poorly coupled to the change in the electronic distribution during excitation. The band due to the $H_g(8)$ mode at 1570 cm^{-1} is obscured by a benzene solvent band. This band is not obscured in CS_2. However, as the electronic absorption band being probed by the laser line is red-shifted in CS_2 relative to benzene, different resonance conditions exist.

The band due to the $A_g(2)$ pentagonal pinch mode has the greatest absolute intensity of all of the C_{60} Raman bands when the LUMO is populated upon resonance with the A electronic state. Its intensity in this excitation region is over three times that of the band due to the $A_g(1)$ mode, whereas inspection of the normal Raman spectra of C_{60} in a number of papers reveals that this factor is about 2.[8,13,17,31−34] The Raman scattering intensity of a band is dependent upon the change in the electronic distribution of the molecule along the coordinates of that vibrational mode, indicating that the change in electronic distribution is more closely associated with the $A_g(2)$ mode than with the $A_g(1)$ mode. It is well documented that upon population of the LUMO of C_{60} in fullerides, the energy of the $A_g(2)$ vibration decreases by ∼6 cm^{-1} per added electron,[5,21,35] but a similar behavior is not observed for the band of the $A_g(1)$ mode.[21] This suggests that the coordinates of the $A_g(2)$ mode are more closely associated with the LUMO molecular orbital than those of the $A_g(1)$ mode. The same relationship is expected upon population of the LUMO by excitation and may be augmented by the creation of the electron hole in the HOMO. The greater electron density associated with the change in the electronic distribution of the molecule along the coordinates of the $A_g(2)$ vibrational mode is reflected in the greater intensity enhancement of the band due to the $A_g(2)$ mode compared to that for the $A_g(1)$ mode.

The bands due to the $H_g(1)$ and $G_g(4)$ modes receive their intensities through B-term scattering upon resonance with the A electronic state. Theoretically, the band due to the $H_g(1)$ mode can gain Raman intensity through Jahn−Teller distortions.[26,36,37] The band due to the $H_g(7)$ mode, however, receives its intensity through a nonadiabatic vibronic coupling mechanism because the energy of this vibration is close to the energy separation of the excited states that it couples.[6] These three modes and related enhancement mechanisms are discussed later.

A characteristic of B-term scattering is that the band intensity of the coupling modes are equal at 0−0 and 0−1 peak resonances. Table 1 gives the ratios of the band intensities at 0−1 and 0−0 resonances. Before discussion of these values can be made, it is noted that the 406.7- and 413.1-nm excitations are not resonant with the maximum absorbances of the 0−1 and 0−0 transitions of the A electronic state, respectively (Figure 5). Further, the 406.7-nm line is also slightly in resonance with the 0−0 transition. It is estimated that these two considerations result in up to a ∼20% deviation from unity for these ratios.[6] Thus, the bands due to the $H_g(1)$, $G_g(4)$, $A_g(1)$, and $A_g(2)$ modes, within these experimental parameters, obey the requirement. For

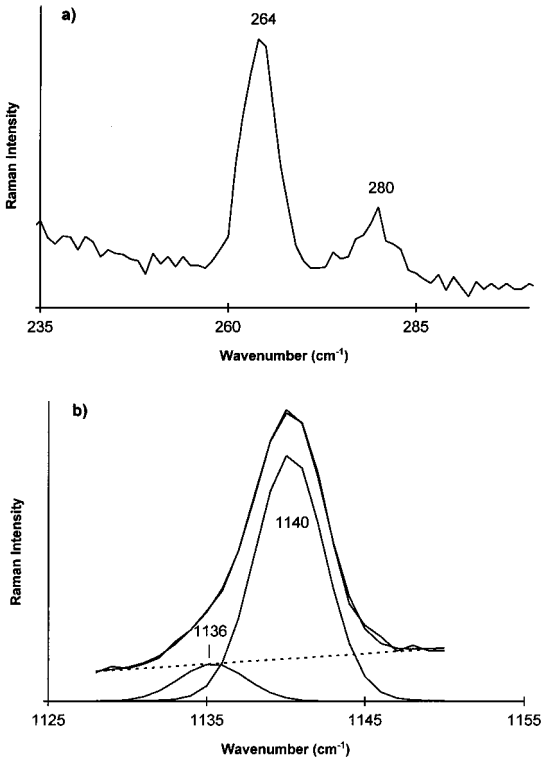

Figure 6. Selected wavenumber regions of the CS_2 solution RR spectrum of C_{60}: (a**)** splitting of the $H_g(1)$ mode into two bands at 264 and 280 cm^{-1}; (b**)** deconvolution of the vibrational envelope of the $G_g(4)$ fundamental mode at 1140 cm^{-1}, revealing a small band at 1136 cm^{-1}.

the $H_g(1)$ vibrational band, however, the intensity behavior is unusual. At 406.7-nm excitation only, the $H_g(1)$ band at 264 cm^{-1} is split (Figure 6), with another band arising at 280 cm^{-1}.[1] This observation can be explained in terms of solvent effects. As with the ground state, the symmetry of the excited state is also lowered from I_h, as will be discussed later. Resonance with the 0−1 transition ($H_g(1)$) at ∼406.5 nm involves excitation of the $H_g(1)$ vibration, which produces a radial distortion of the molecule. The symmetry distortion of C_{60} in the excited state due to solvent interactions is likely to be dynamic. The two distortions may not necessarily occur along the same coordinates, and hence, the degeneracy of the $H_g(1)$ mode could be removed. This vibrational excitation does not occur at 0−0 resonance, and the band of the $H_g(1)$ mode retains its integrity. Further, the intensity of this band at 280 cm^{-1} accounts for the lower intensity of the 264 cm^{-1} band at 0−1 resonance compared to 0−0 resonance.

Of the five REPs, the $H_g(7)$ mode is the obvious outlier with a band intensity at 0−1 resonance over four times greater than that at 0−0 resonance. This is a manifestation of the rare D-term or nonadiabatic scattering mechanism in C_{60}, communicated earlier by us.[6] The experimental value for the ratio of the intensities of the band of the $H_g(7)$ mode at 0−1 and 0−0 is 4.2 ± 0.8, compared with the calculated value of 2.9 from the "no-Jahn−Teller nonadiabatic coupling prediction," given by the ratio[6,27]

$$\frac{I_{0-1}}{I_{0-0}} = \left(\frac{\Delta\nu_{es} + \nu_k}{\Delta\nu_{es} - \nu_k}\right)^2 \qquad (5)$$

where I_{0-1} and I_{0-0} are the intensities of a vibrational band, k, at 0−1 and 0−0 resonances, respectively. The term $\Delta\nu_{es}$ is the electronic energy spacing (cm^{-1}) between the two coupled electronic excited states, and the ν_k term is the energy of the vibration (cm^{-1}). The calculated value is outside the experimental error for the empirical value, but this discrepancy may be explained in symmetry terms. As reported earlier,[1,6] the band due to the $H_g(7)$ vibrational mode is split in the solution spectrum due to solvent effects—there are at least two bands under this vibrational envelope. Given that the symmetry of C_{60} in solution is slightly reduced, the efficacy of each of the three vibrational modes in coupling the electronic excited states may differ. Nonetheless, this result indicates that the Jahn−Teller distortion of the excited state of C_{60} (C_{60}*) along the coordinates of the $H_g(7)$ mode is small, if not negligible, as any Jahn−Teller activity of this mode would be manifested as an empirical value *smaller* than that for the theoretical prediction.[27] The presence of the band due to the first overtone mode of $H_g(7)$ in the RR spectra at 2845 cm^{-1} also suggests D-term scattering (Figure 4).[28] The $H_g(8)$ band at 1570 cm^{-1} should also be a good candidate for D-term activity, but in benzene this band is completely obscured due to solvent band coincidence. In CS_2, the transition envelopes are shifted due to solvatochromism[38] and the 0−0 and 0−1 transitions are no longer in the same positions relative to the 413.1- and 406.7-nm laser lines. However, no band is evident at ∼3140 cm^{-1} for the predicted $2H_g(8)$ overtone mode.

It is now well-established that the symmetry of C_{60} is sensitive to its solvent environment, especially evident for fast time scale experiments.[1,2] This is evidenced by the removal of the degeneracy of the non-totally-symmetric H_g modes and the proliferation of bands arising from IR-active/Raman-silent and IR/Raman-silent vibrational modes.[1,6] The probable mechanism for the symmetry lowering is the increase in effective rotating volume of C_{60} that arises in electron-donating solvents.[2] All of the bands of modes that are activated due to the relaxation of the Raman selection rules have weak intensities upon resonance with the A electronic state, except for the band of the IR/Raman-silent $G_g(4)$ mode at 1140 cm^{-1}. The intensity behavior exhibited by the latter vibration and its extensive involvement in the RR spectra are unusual.

The $G_g(4)$ band was assigned using both the published inelastic electron tunneling spectrum of C_{60} and theoretical data.[1,39,40] Dong *et al.*[11] reported a band at ∼1140 cm^{-1} and gave at least two possibilities for the assignment.[41] These included the $H_g(2) + H_g(3)$ combination mode and the A_u fundamental mode. It is unlikely that this band arises from a combination mode as its band intensity is greater than all but the most intense fundamental modes, including the suggested component $H_g(2)$ and $H_g(3)$ fundamental modes. It is also unlikely that the A_u assignment is correct for two reasons: an ungerade mode is not of the correct symmetry to vibronically couple the ungerade electronic excited states, and closer inspection of the band reveals that it is split with a smaller band at 1136 cm^{-1} contributing to the asymmetry at lower energy (Figure 6). It could be argued that the band at 1136 cm^{-1} is due to the proposed combination mode, but its intensity is comparable to the intensities of the bands for the proposed component fundamental modes; therefore, we deduce that it is a component of the $G_g(4)$ band, which is split due to symmetry reduction.

From work carried out on the solvent effects on the electronic spectrum of C_{60},[38] there is evidence that the symmetry of C_{60}* is related to that of C_{60}^{1-}. Koga and Morokuma[36] have calculated the structure of the monoanion under D_{5d}, D_{2h}, and D_{3d} symmetries, and our recent analysis of the NIR spectrum of C_{60}^{1-} has endorsed the adequacy of any of these models.[42] The intensity enhancement of the $G_g(4)$ vibration in the RR spectra of C_{60} in this work, however, is suggestive of D_{5d}

TABLE 3: Correlations of the t_{1u} Electronic and g_g Vibrational Symmetries of I_h Point Group with D_{5d}, D_{2h}, and D_{3d} Point Groups[a]

I_h point group	t_{1u} electronic	g_g vibrational
D_{5d}	$a_{2u} + e_{1u}$	e_{1g} (>2) + e_{2g} (0.75)
D_{2h}	$b_{1u} + b_{2u} + b_{3u}$	b_{1g} (>2) + b_{2g} (>2) + b_{3g} (>2)
D_{3d}	$a_{2u} + e_u$	a_{2g} (∞) + e_g (>2)

[a] The parenthesized values correspond to the on-resonance depolarization ratios of that orbital symmetry.

symmetry for C_{60}*. Table 3 gives the correlations of the I_h point group with D_{5d}, D_{2h}, and D_{3d} point groups for the G_g vibrational and the T_{1u} electronic symmetries. The predicted on-resonance depolarization ratio for the band of each non-totally symmetric mode is parenthesized. The depolarization ratio for the band arising from the $G_g(4)$ vibrational mode in I_h symmetry was $\rho(\pi/2) = 0.6 \pm 0.05$. For a non-totally-symmetric mode, an experimental value of $\rho(\pi/2) = 0.6$ can only correspond to an E_{2g} vibration in the D_{5d} symmetry point group. Thus, the symmetry correlations in Table 3 indicate that D_{5d} is the best approximation to the symmetry of C_{60}*. In D_{5d}, the T_{1u} LUMO and the excited states of other allowed electronic transitions, split into $A_{2u} + E_{1u}$ pairs. From group theory for vibronic coupling, an E_{2g} vibration can couple the excited states of e_{1u} orbital symmetry in a solvent-distorted C_{60}. Independently, Jeoung *et al.*[43] have attributed new bands arising in the triplet-state Raman spectra of C_{60} in toluene solution to symmetry reduction in the electronic excited state. While depolarization ratios indicate that the symmetry of the distorted excited state can be approximated to the D_{5d} point group, the I_h point group remains the best descriptor for the 10 fundamental Raman modes of C_{60}.

Resonance with the ϵ Electronic State. B-term scattering mechanisms are also expected to be responsible for any resonance effects associated with symmetry-forbidden transitions.[29] The Herzberg−Teller active vibrational modes for the ϵ electronic state have t_{1g}, t_{2g}, g_g, and h_g symmetries,[26,37] on the basis of the tentative assignment of Leach *et al.*[26] In terms of RR scattering, modes active in vibronic coupling will have their band intensities enhanced.[28] Given that the ϵ electronic state is energetically well-removed from the strongly-allowed electronic transitions by >10 000 cm^{-1}, vibronic coupling will be small. This is evidenced by the weak intensities of the bands due to the $H_g(1)$, $A_g(1)$, and $A_g(2)$ modes and the negligible intensities for those of the $G_g(4)$ and $H_g(7)$ modes upon resonance with the ϵ electronic state. The activity of the A_g modes in this region has two possible explanations. The reduction of symmetry of C_{60} in solution may allow the A_g modes to become Herzberg−Teller active, and/or the assignment of the electronic spectrum in this region requires reinvestigation. Reduction of symmetry from solute−solvent interactions was not considered by Leach *et al.*[26] when determining the activation of these orbitally-forbidden electronic bands. Such solvent effects may also explain the relative high intensities of these electronic transitions.

Comments on Possible Raman Scattering Mechanisms Due to Jahn−Teller Distortions. It has been reported that RR spectroscopy is the most sensitive technique for probing Jahn−Teller distortions of electronic excited states.[44] Jahn−Teller activity arises from the intramanifold coupling in the resonant Jahn−Teller distorted excited state[29,30,44,45] in which the Born−Oppenheimer approximation breaks down completely. Jahn−Teller active vibrational modes are expected to be especially active in the RR scattering,[29] and this is manifested in three ways. A Jahn−Teller active mode has a large band intensity enhancement upon resonance with the degenerate excited state; it has appreciable intensity off resonance,[44] and one quantum of this mode appears in combination band progressions with *quanta* of totally-symmetric modes.[28]

The T_{1u} LUMO of C_{60} should have its degeneracy lifted by a Jahn−Teller distortion.[26,36,37] The degeneracy is removed by excitation of vibrations of appropriate symmetry, which for C_{60} are of H_g symmetry. On the basis of theoretical calculations, the $H_g(1)$ mode is the most active mode for Jahn−Teller activity in the RR spectrum.[46] For C_{60} in the gas phase, the distortion of the T_{1u} electronic state due to Jahn−Teller distortion would only be expected to be small given the size and structure of the molecule (see above); hence ΔQ would be correspondingly small, and any A-term scattering arising from this overlap would be minimal.

As discussed above, the band of the $H_g(1)$ mode receives intensity enhancement via a B-term mechanism at resonance with the A electronic state. Any A-term scattering that may arise from Jahn−Teller activity would interfere destructively with the B-term contribution and would be manifested as a significantly lower intensity of the JT-active band at 0−1 resonance compared to 0−0 resonance.[28] Off resonance at 647.1-nm excitation, a very weak band appears at 264 cm^{-1}, just above the noise. While this may indicate JT activity, the JT inactive $A_g(1)$ vibrational band has approximately equal intensity at this excitation. Even for a small Jahn−Teller effect, combination band progressions of the Jahn−Teller active $H_g(1)$ mode with quanta of totally-symmetric modes are expected.[28] Their absence in the RR spectrum of C_{60} strongly suggests that any Jahn−Teller distortion of the T_{1u} LUMO is less important than solvent-induced distortions; *i.e.*, the solute−solvent interaction has, to a large extent, already facilitated the removal of the degeneracy of the T_{1u} LUMO through the lowering of the symmetry of C_{60}. The lack of significant Raman scattering mechanisms due to Jahn−Teller distortions provides strong supporting evidence of our earlier assertions on the importance of solvent effects on lowering the symmetry of C_{60} and C_{60}*.

Overtones and Combination Bands of Herzberg−Teller Active Modes. As discussed earlier, the 0−1 vibronic sideband gains its intensity by Herzberg−Teller coupling. Owing to the solvatochromism displayed by C_{60},[38,47] the 413.1-nm exciting line is in resonance with the 0−0 transition of C_{60}, which occurs at 414.0 nm in CS_2, but it is also partially in resonance with the 0−1 transition. For C_{60}, the appearance of *first* overtones and combinations in the RR spectrum involving the A_g, H_g, and G_g Herzberg−Teller active modes is indicative of a second-order Herzberg−Teller coupling process.[27,30] Theoretical calculations of Negri *et al.*[46] predict only short vibrational progressions for C_{60}. The bands due to overtones and combinations of C_{60} involving more than two quanta are not observed, which is consistent with the absence of a 0−2 transition envelope in the electronic absorption spectrum. The second-order Herzberg−Teller coupling explains the appearance of bands due to the overtones $2A_g(1)$ at 976 cm^{-1} and $2A_g(2)$ at 2940 cm^{-1}, and combinations of A_g and H_g modes. The band due to the $2H_g(7)$ overtone mode at 2845 cm^{-1} most likely arises from a D-term mechanism, discussed earlier. The unusual observation of a band arising from an overtone of an IR/Raman-silent mode, $2G_g(4)$ at 2283 cm^{-1}, and of combinations involving Raman-inactive modes may also be explained in terms of a second-order Herzberg−Teller coupling of these modes becoming Raman-activated from solvent-induced symmetry lowering.

The presence of bands arising from overtone and combination progression modes provides information on the extent of the anharmonicity. It has been suggested, by at least one group,

that the anharmonicity of C_{60} should be quite large.[48] However, the close agreement (<4 cm^{-1}) with the predicted combination and overtone band wavenumbers, based on the fundamental wavenumbers for the component modes and the observed wavenumbers in this work and by others,[11] shows that the anharmonicity in the spectroscopy of C_{60} is quite small. This is consistent with the rigid nature of the molecule.

Implications of the RR Spectroscopy of C_{60}. *(a) Superconductivity.* This property of alkali-metal-doped C_{60} fullerides, of the form A_3C_{60} (where A is an alkali metal), is perhaps the most exciting and promising application of C_{60} at present.[22,23] Indeed, the superconducting ability of these fullerene materials is only surpassed by the copper oxide-based ceramics. The valence band and the conduction band of the solid state are derived from the HOMO and LUMO of C_{60}, respectively. Given that both the electronic states and the intramolecular phonons in A_3C_{60} are little changed from molecular C_{60},[21,23,49] and, as revealed above, the symmetry of the excited state of C_{60} in solution is closer to the symmetry of the fullerides than of C_{60} in the gas phase, the RR spectroscopic behavior of C_{60} may provide useful insights into the dynamics of superconductivity.

One of the most discussed issues is the question of the electron-phonon coupling, which is integral to the superconductivity. The favored theories have the electron pairing being driven mainly by intramolecular vibrations,[49−52] especially the high-energy modes.[53] The t_{1u} symmetry of the LUMO of I_h C_{60} dictates that only phonons with a_g or h_g symmetry can couple with the orbital, but only the H_g modes are predicted to couple strongly.[22]

At least four theory papers have predicted that the $H_g(7)$ mode should be the most active intramolecular vibration in the superconducting electron−phonon coupling.[50,51,54,55] If this mode is involved, the applicability of the Born−Oppenheimer approximation (Migdal's theorem) is brought into question as the closeness in energy of the band of this mode and the Fermi energy implicates nonadiabaticity.[21] The REP calculations for C_{60} confirm that the $H_g(7)$ mode is involved in *nonadiabatic* vibronic coupling of t_{1u} orbitals,[6] strongly supporting the efficacy of the $H_g(7)$ mode's involvement in the superconducting pairing mechanism. Some authors believe that the $H_g(8)$ mode may also be important in this regard. While it is not possible to examine D-term scattering mechanisms in benzene because of solvent band coincidences, the absence of a band due to the $2H_g(8)$ overtone mode indicates that unlike the $H_g(7)$ mode, the $H_g(8)$ mode does not undergo appreciable D-term scattering. This, in turn, supports the notion that nonadiabatic vibronic coupling involving the $H_g(7)$ mode is more likely to be involved in the pairing mechanism of superconductivity than the $H_g(8)$ mode.

(b) HIV-1 Protease Association Mechanism. The combination of Raman-activation of silent modes and the removal of degeneracy of Raman-active modes arising from a solvent-induced distortion illustrates the sensitivity of C_{60} to its environment and shows that these solvent interactions with C_{60} are significant. These interactions probably occur through donation of solvent electron density to C_{60} via the enlarged external pπ lobes at each carbon. This is particularly pronounced for aromatic solvents where the interaction is expected to occur through a π-stacking arrangement. It is possible that similar C_{60}/aromatic interactions with the hydrophobic aromatic amino acids, including phenylalanine, tyrosine, and tryptophan, in the pocket of HIV-1 protease[56] are important in the strong binding of C_{60} to the enzyme, giving derivatives their anti-HIV activities.

Summary and Conclusion

The REP constructions for C_{60} at seven laser excitations between 514.5 and 406.7 nm reveal that resonance conditions exist across this region. This highlights the inadequacies of many papers where the resonance conditions of the experiment have been neglected. Upon resonance with the A electronic state, the bands due to the A_g and H_g vibrational modes receive resonance Raman intensity through adiabatic vibronic coupling mechanisms, except for the $H_g(7)$, which is involved in a nonadiabatic mechanism. There is no evidence for scattering intensity enhancement mechanisms due to Jahn−Teller interactions. At resonance with the ϵ electronic state, B-term scattering mechanisms operate. The intensity of A_g vibrational bands due to excitation in this region implies that the ϵ electronic state assignments of Leach *et al.*[26] may require reconsideration. The lower symmetry of solvated C_{60} may also account for the unusually high relative intensity of these forbidden electronic transitions.

The RR spectrum of C_{60} in solution displays almost the full gamut of RR vibrational phenomena, more than any other individual molecule or complex. These include the unusual observation of resonance enhancement of an overtone band of an IR/Raman-silent mode and combination bands involving an IR/Raman-silent mode with totally-symmetric, non-totally-symmetric, and IR-active/Raman-silent modes. These numerous features have their origin in the relaxation of Raman selection rules caused by a reduction of the high symmetry of C_{60} in the solvent environment. The intensity behavior and depolarization ratio of the band of the Raman-silent $G_g(4)$ mode at 1140 cm^{-1} indicate that D_{5d} is the best approximation for the symmetry of the excited state of C_{60}. This also suggests that the integrity of the I_h symmetry of proposed giant fullerenes, C_{240} and C_{540},[57] would be extremely sensitive to environmental perturbations. An interesting manifestation of the rotating solute−solvent complex is that the resulting lower symmetry removes the degeneracy of the resonant T_{1u} LUMO thereby eliminating the need to invoke Jahn−Teller distortion. Further, the lower symmetry of C_{60} in solution may partially account for its greater than expected reactivity.

These results, taken with those obtained for C_{70},[7,58] provide compelling evidence that extensive intersystem mixing (HT and nonadiabatic) is an important feature of the spectroscopy of fullerenes. Fullerenes are certainly rewarding subjects for investigations of symmetry and vibronic coupling, especially in solvent environments. Our work has demonstrated that RR spectra of C_{60} and C_{70} are rich in information on symmetry, electronic degeneracy, and vibronic coupling. Systematic studies of larger fullerenes should prove to be equally rewarding, with fullerenes possibly challenging the porphyrins as the nearly ideal class of molecules in which to study RR scattering phenomena.

Acknowledgment. The authors are grateful for support from the Australian Postgraduate Award Scheme (S.H.G.), the Australian Research Council (R.S.A. and P.A.L.) and the National Institutes of Health (GM 23851) (C.A.R.), and to Dr. J. R. Reimers for helpful discussions and Dr. B. M. Collins for help with the calibration of data and REP calculations.

References and Notes

(1) Gallagher, S. H.; Armstrong, R. S.; Lay, P. A.; Reed, C. A. *Chem. Phys. Lett.* **1996**, *248*, 353.

(2) Rubstov, I. V.; Khudiakov, D. V.; Nadtochenko, V. A.; Lobach, A. S.; Moravskii, A. P. *Chem. Phys. Lett.* **1994**, *229*, 517.

(3) Matus, M.; Kuzmany, H.; Krätschmer, W. *Solid State Commun.* **1991**, *80*, 839.

(4) Sinha, K.; Menendez, J.; Hanson, R. C.; Adams, G. B.; Page, J. B.; Sankey, O. F.; Lamb, L. D.; Huffman, D. R. *Chem. Phys. Lett.* **1991**, *186*, 287.

(5) McGlashen, M. L.; Blackwood, M. E., Jr.; Spiro, T. G. *J. Am. Chem. Soc.* **1993**, *115*, 2074.

(6) Gallagher, S. H.; Armstrong, R. S.; Lay, P. A.; Reed, C. A. *J. Am. Chem. Soc.* **1994**, *116*, 12091.

(7) Gallagher, S. H.; Armstrong, R. S.; Lay, P. A.; Reed, C. A. *Chem. Phys. Lett.* **1995**, *234*, 245.

(8) Lynch, K.; Tanke, C.; Menzel, F.; Brockner, W.; Scharff, P.; Stumpp, E. *J. Phys. Chem.* **1995**, *99*, 7985.

(9) Brockner, W.; Menzel, F. *J. Mol. Struct.* **1996**, *378*, 147.

(10) Gallagher, S. H.; Armstrong, R. S.; Bolskar, R. D.; Lay, P. A.; Reed, C. A. *J. Mol. Struct.*, in press.

(11) Dong, Z.-H.; Zhou, P.; Holden, J. M.; Eklund, P. C.; Dresselhaus, M. S.; Dresselhaus, G. *Phys. Rev. B* **1993**, *48*, 2862.

(12) Gallagher, S. H.; Armstrong, R. S.; Lay, P. A.; Reed, C. A. *J. Raman Spectrosc.*, in press.

(13) Bethune, D. S.; Meijer, G.; Tang, W. C.; Rosen, H. J.; Golden, W. G.; Seki, H.; Brown, C. A.; de Vries, M. S. *Chem. Phys. Lett.* **1991**, *179*, 181.

(14) Meilunas, R.; Chang, R. P. H.; Liu, S.; Jensen, M.; Kappes, M. M. *J. Appl. Phys.* **1991**, *70*, 5128.

(15) Eklund, P. C.; Zhou, P.; Wang, K.-A.; Dresselhaus, G.; Dresselhaus, M. S. *J. Phys. Chem. Solids* **1992**, *53*, 1391.

(16) Akers, K. L.; Douketis, C.; Haslett, T. L.; Moskovits, M. *J. Phys. Chem.* **1994**, *98*, 10824.

(17) Dresselhaus, M. S.; Dresselhaus, G.; Eklund, P. C. *J. Raman Spectrosc.* **1996**, *27*, 351.

(18) Akselrod, L.; Byrne, H. J.; Thomsen, C.; Mittelbach, A.; Roth, S. *Chem. Phys. Lett.* **1993**, *212*, 384.

(19) Lopinski, G. P.; Fox, J. R.; Lannin, J. S. *Chem. Phys. Lett.* **1995**, *239*, 107.

(20) Bowmar, P.; Hayes, W.; Kurmoo, M.; Pattenden, P. A.; Green, M. A.; Day, P.; Kikuchi, K. *J. Phys.: Condens. Matter* **1994**, *6*, 3161.

(21) Haddon, R. C. *Acc. Chem. Res.* **1992**, *25*, 127.

(22) Rosseinsky, M. J. *J. Mater. Chem.* **1995**, *5*, 1497.

(23) Tanigaki, K.; Prassides, K. *J. Mater. Chem.* **1995**, *5*, 1515.

(24) Bio-Rad WIN-IR Version 2.04 based on GRAMS/386, Galactic Industries Corp.; 1991.

(25) Atkins, P. W. *Physical Chemistry*, 4th ed.; Oxford University Press: Suffolk, 1990.

(26) Leach, S.; Vervloet, M.; Desprès, A.; Bréheret, E.; Hare, J. P.; Dennis, T. J.; Kroto, H. W.; Taylor, R.; Walton, D. R. M. *Chem. Phys.* **1992**, *160*, 451.

(27) Rousseau, D. L.; Friedman, J. M.; Williams, P. F. *Topics in Current Physics*; Weber, A., Ed.; Springer-Verlag: Berlin, Heidelberg, New York, 1979; pp 203.

(28) Clark, R. J. H.; Dines, T. J. *Angew. Chem., Int. Ed. Engl.* **1986**, *25*, 131

(29) Spiro, T. G.; Stein, P. *Annu. Rev. Phys. Chem.* **1977**, *28*, 501.

(30) Clark, R. J. H.; Stewart, B. *Struct. Bond. (Berlin)* **1979**, *36*, 1.

(31) Dennis, T. J.; Hare, J. P.; Kroto, H. W.; Taylor, R.; Walton, D. R. M. *Spectrochim. Acta, Sect. A* **1991**, *47A*, 1289.

(32) Garrell, R. L.; Herne, T. M.; Szafranski, C. A.; Diederich, F.; Ettl, F.; Whetten, R. L. *J. Am. Chem. Soc.* **1991**, *113*, 6302.

(33) Chase, B.; Fagan, P. J. *J. Am. Chem. Soc.* **1992**, *114*, 2252.

(34) Love, S. P.; McBranch, D.; Salkola, M. I.; Coppa, N. V.; Robinson, J. M.; Swanson, B. I.; Bishop, A. R. *Chem. Phys. Lett.* **1994**, *225*, 170.

(35) Haddon, R. C.; Hebard, A. F.; Rosseinsky, M. J.; Murphy, D. W.; Duclos, S. J.; Lyons, K. B.; Miller, B.; Rosamilia, J. M.; Fleming, R. M.; Kortan, A. R.; Glarum, S. H.; Makhija, A. V.; Muller, A. J.; Eick, R. H.; Zahurak, S. M.; Tycko, R.; Dabbagh, G.; Thiel, F. A. *Nature* **1991**, *350*, 320.

(36) Koga, N.; Morokuma, K. *Chem. Phys. Lett.* **1992**, *196*, 191.

(37) Yabana, K.; Bertsch, G. F. *Chem. Phys. Lett.* **1992**, *197*, 32.

(38) Gallagher, S. H.; Armstrong, R. S.; Lay, P. A.; Reed, C. A. *J. Phys. Chem.* **1995**, *99*, 5817. Armstrong, R. S.; Gallagher, S. H.; Lay, P. A.; Reed, C. A.; Reimers, J. R. *J. Phys. Chem.* **1996**, *100*, 5604.

(39) Brousseau, J.-L.; Tian, K.; Gauvin, S.; Leblanc, R. M.; Delhaes, P. *Chem. Phys. Lett.* **1993**, *202*, 521.

(40) In addition, D. A. Dixon, B. E. Chase, G. Fitzgerald, and N. Matsuzawa at http://www.cray.com/PUBLIC/APPS/UNICHEM/examples/c60/c60.vib.html used LSD calculations to predict the energy (cm^{-1}) of the $G_g(4)$ mode to be 1122 cm^{-1}.

(41) Dong *et al.*[11] indicated that there were three other possibilities of combination modes within 3 cm^{-1} of the band, but they were not identified.

(42) Bolskar, R.; Gallagher, S. H.; Armstrong, R. S.; Lay, P. A.; Reed, C. A. *Chem. Phys. Lett.* **1995**, *247*, 57.

(43) Jeoung, S. C.; Kim, D.; Kim, S.; Kim, S. K. *Chem. Phys. Lett.* **1995**, *241*, 528.

(44) Muramatsu, S.; Nasu, K.; Takahashi, M.; Kaya, K. *Chem. Phys. Lett.* **1977**, *50*, 284.

(45) Shelnutt, J. A.; Cheung, L. D.; Chang, R. C. C.; Yu, N.-T.; Felton, R. H. *J. Chem. Phys.* **1977**, *66*, 3387.

(46) Negri, F.; Orlandi, G.; Zerbetto, F. *Chem. Phys. Lett.* **1988**, *144*, 31−37.

(47) Bensasson, R. V.; Bienvenue, E.; Dellinger, M.; Leach, S.; Seta, P. *J. Phys. Chem.* **1994**, *98*, 3492.

(48) Chase, B.; Herron, N.; Holler, E. *J. Phys. Chem.* **1992**, *96*, 4262.

(49) Gunnarsson, O.; Handschuh, H.; Bechthold, P. S.; Kessler, B.; Ganteför, G.; Eberhardt, W. *Phys. Rev. Lett.* **1995**, *74*, 1875.

(50) Varma, C. M.; Zaanen, J.; Raghavachari, K. *Science* **1991**, *254*, 989.

(51) Schluter, M.; Lannoo, M.; Needels, M.; Baraff, G. A.; Tomanek, D. *Phys. Rev. Lett.* **1992**, *68*, 526.

(52) Zhou, O.; Fleming, R. M.; Murphy, D. W.; Rosseinsky, M. J.; Ramirez, A. P.; van Dover, R. B.; Haddon, R. C. *Nature* **1993**, *362*, 433.

(53) Prassides, K.; Tomkinson, J.; Christides, C.; Rosseinsky, M. J.; Murphy, D. W.; Haddon, R. C. *Nature* **1991**, *354*, 462.

(54) Faulhaber, J. C. R.; Ko, D. Y. K.; Briddon, P. R. *Phys. Rev. B* **1993**, *48*, 661.

(55) Antropov, V. P.; Gunnarsson, O.; Liechtenstein, A. I. *Phys. Rev. B* **1993**, *48*, 7651.

(56) Friedman, S. H.; DeCamp, D. L.; Sijbesma, R. P.; Srdanov, G.; Wudl, F.; Kenyon, G. L. *J. Am. Chem. Soc.* **1993**, *115*, 6506.

(57) Scuseria, G. E. *Chem. Phys. Lett.* **1995**, *243*, 193.

(58) Gallagher, S. H.; Armstrong, R. S.; Bolskar, R. D.; Lay, P. A.; Reed, C. A. *J. Am. Chem. Soc.*, in press.